Energy and AI 14 (2023) 100275

Contents lists available at ScienceDirect

Energy and AI

journal homepage: www.sciencedirect.com/journal/energy-and-ai

Mathematical modeling of fuel cells fed with an electrically rechargeable liquid fuel

Xingyi Shi [a], Xiaoyu Huo [a], Oladapo Christopher Esan [a], Zhefei Pan [a], Liu Yun [a], Liang An [a,b,*], T.S. Zhao [c,*]

[a] Department of Mechanical Engineering, The Hong Kong Polytechnic University, Hung Hom, Kowloon, Hong Kong SAR, China
[b] Research Institute for Smart Energy (RISE), The Hong Kong Polytechnic University, Hung Hom, Kowloon, Hong Kong SAR, China
[c] Department of Mechanical and Aerospace Engineering, The Hong Kong University of Science and Technology, Clear Water Bay, Kowloon, Hong Kong SAR, China

HIGHLIGHTS

- A mathematical model is developed for a passive fuel cell fed with an e-fuel.
- The simulation results are in a great agreement with the experimental data.
- The effects of various structural and operating conditions are examined.
- The concentration distribution of reactive species inside the cell is presented.

GRAPHICAL ABSTRACT

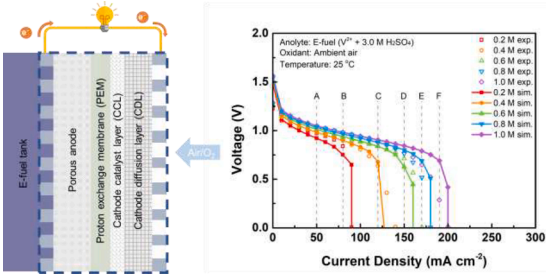

ARTICLE INFO

Keywords:
E-fuel
Mathematical modeling
Liquid fuel cells
Structural parameters
Operation conditions

ABSTRACT

Lately, utilizing a novel electrically rechargeable liquid fuel (e-fuel), a fuel cell has been designed and fabricated, which is demonstrated to achieve a much better performance than alcoholic liquid fuel cells do. However, its current performance, which thus hampers its wide application, demands further improvement to meet up with industrial requirement. Therefore, to attain a better performance for this system, an in-depth understanding of the complex physical and chemical processes within this fuel cell is essential. To this end, in this work, a two-dimensional transient model has been developed to gain an extensive knowledge of a passive e-fuel cell and analyze the major factors limiting its performance. The effects of various structural parameters and operating conditions are studied to identify the underlying performance-limiting factors, where deficient mass transport is found to be one of the major causes. The increment of anode porosity and thickness are found to be effective methods of improving the cell performance. This study therefore provides insights on achieving further performance advancement of the fuel cell in the future.

1. Introduction

In recent decades, due to the growing needs for energy across the globe, the search for sustainable energy sources to replace the traditional fossil fuels has attracted increasing attention [1–3]. To date, diverse kinds of novel power generation systems have been developed, among which the proton exchange membrane fuel cell (PEMFC),

* Corresponding authors.
E-mail addresses: liang.an@polyu.edu.hk (L. An), metzhao@ust.hk (T.S. Zhao).

https://doi.org/10.1016/j.egyai.2023.100275

Available online 2 June 2023

Nomenclature

a_v	Specific area, m^{-1}
C	Species concentration, mol m^{-3}
D	Diffusion coefficient, $m^2\ s^{-1}$
E	Potential/voltage, V
E^0	Equilibrium potential, V
F	Faradic constant, A s mol^{-1}
h	Cell height, m
i	Current density, A m^{-3}
i_0	Exchange current density, A m^{-2}
k	Reaction rate constant, m s^{-1}
$\overrightarrow{N}$	Flux, mol $m^{-2}\ s^{-1}$
n	Number of participating electrons
$\overrightarrow{n}$	Normal vector
R	Universal gas constant, J $mol^{-1}\ K^{-1}$
S	Source term
T	Operating temperature, K
t	Time, s
u	Mobility, mol s kg^{-1}
v	Stoichiometric coefficient
w	Cell width, m
z	Valence of ion

Greek

α	Charge transfer coefficient
γ	Reaction order
δ	Thickness, m
ε	Porosity
η	Overpotential, V
σ	Conductivity, S m^{-1}
ϕ	Potential, V

Superscripts

0	Initial
ccl	Cathode catalyst layer
eff	Effective
ref	Reference

Subscripts

a	Anode
c	Cathode
ccl	Cathode catalyst layer
cdl	Catalyst diffusion layer
H^+	Proton
i	Species
l	Liquid
m	Membrane
O_2	Oxygen
s	Solid
SO_4^{2-}	Sulphate ion
V^{2+}	Vanadium (II) ion
V^{3+}	Vanadium (III) ion

employing hydrogen as fuel, has received great attention [4,5]. However, hampered by the difficulties of hydrogen production, storage, and transportation, the widespread adoption of PEMFCs is still being restricted [6,7]. As an alternative, liquid fuel cells using alcohol fuels instead of hydrogen is believed to be a promising candidate [4,8,9]. While liquid fuel cells avoid the difficulties associated with the handling of gaseous fuels, their limited performance become the major barriers in their commercialization process [10,11].

Recently, an innovative fuel cell using an electrically rechargeable liquid fuel (e-fuel) has attracted research attentions worldwide [12]. Compared with the conventional direct liquid fuel cells utilizing hydrogen or alcohol fuels, the e-fuel solution that can be made of a wide range of electroactive materials are recyclable and rechargeable. In our previous study, we have developed a liquid fuel cell using the e-fuel containing vanadium ions as reactive species and oxygen, and investigated its power generation performance under various operating conditions [13]. While the demonstrated system has presented a superior performance, it is believed that there remains a large room for further performance improvement in the future. Therefore, it is necessary to gain an in-depth insight on the complex physical and chemical processes which occur inside the cell [14]. As a promising solution, mathematical model has demonstrated great potential in analyzing fuel cell systems from a fundamental perspective [15–17]. It is a powerful computational tool that can simulate the processes inside the cell, as well as determining the influence of various structural and operation parameters, such as the reactive species concentrations and electrode porosity [18]. In the past decades, many numerical models have been developed for evaluating the fuel cell systems, including PEMFCs and direct alcoholic liquid fuel cells [19,20]. Detailed studies have also been performed on investigating their mass and charge transport processes (e.g., under-rib convection [21,22]), electrochemical reactions (e.g., mixed potential [23–25]) and cell designs (e.g., flow field design [26–28]). Nevertheless, up till now, there is no computational model for the passive fuel cell fed with the novel e-fuel, confining the in-depth understanding to this system. It is thus pivotal to develop a mathematical model that can simulate these processes in the system under different conditions.

In this work, in order to obtain an in-depth insight into the complex physical and electrochemical processes as well as optimize system design and operation conditions, a two-dimensional transient model is developed for a passive liquid fuel cell fed with the e-fuel. To begin with, the experimental data is compared with the simulation results for validation, which is found to show a good agreement. Thereafter, to illustrate the effects of various structural parameters and operating conditions, the cell performance is simulated by varying the e-fuel compositions, oxygen concentrations, electrode porosity and thickness, as well as exchange current densities. Moreover, to gain an extensive knowledge for the e-fuel cell and analyze the major factors limiting its performance, the concentration distributions of reactive species in the cell are obtained to provide substantial information inside the cell.

2. Model formulation

2.1. Physical and chemical processes

The computational domain of the cell is presented in Fig. 1, comprising of the anode/cathode current collectors, a porous anode, a proton exchange membrane (PEM), and a porous cathode diffusion layer (CDL) coated with cathode catalyst layer (CCL). During the cell operation, the e-fuel would transport from the tank to the anode surface for the oxidation reaction as shown below [12]:

$$\text{Anode}: \quad V^{2+} \rightarrow V^{3+} + e^- \qquad E_a^0 = -0.26\ V \tag{1}$$

The released electrons would then follow the external electrical circuit to reach the cathode side. Meanwhile, the oxidant will diffuse through the CDL to the CCL surface to react with the protons and electrons as [12]:

$$\text{Cathode}: \quad O_2 + 4H^+ + 4e^- \rightarrow 2H_2O \qquad E_c^0 = +1.23\ V \tag{2}$$

The overall reaction can thus be expressed as [12]:

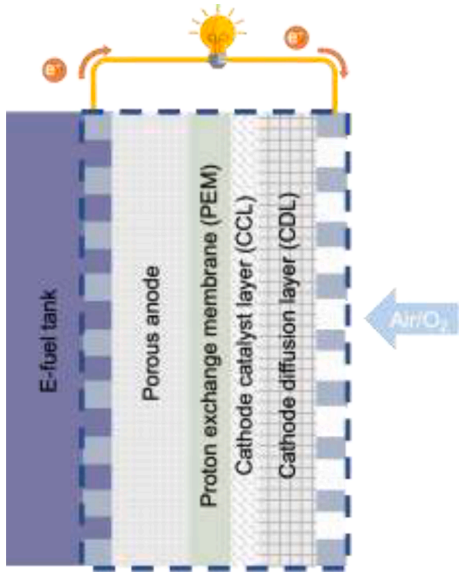

Fig. 1. Schematic of the domain of passive liquid fuel cell.

$$\text{Overall}: \ 4V^{2+} + O_2 + 4H^+ \rightarrow 4V^{3+} + 2H_2O \qquad E^0 = 1.49\ V \tag{3}$$

Therefore, thermodynamically, the theoretical voltage of this cell is as high as 1.49 V, which exceeds that of the convectional alcohol fuel cells and PEMFCs [12].

2.2. Model assumptions

As the properties of components inside the simulated passive fuel cell can be regarded as homogenous along the z-direction, a 2D model is developed to reduce the computational complexity. Furthermore, to simplify the multiple physical and chemical processes occurring inside the cell, the computational 2D model considers the following assumptions:

1) Properties of anode, cathode and membrane are regarded to be homogeneous and isotropic.
2) The crossover of liquid/gas flow across the membrane are neglected.
3) Side reactions are neglected.
4) The liquid water generated during the cell operation is ignored.
5) The two-step dissociation of sulfuric acid is fully completed.

2.3. Governing equations

2.3.1. Anode

2.3.1.1. Mass transport. The mass transport of various species at the anode side mainly follows diffusion and migration. Following the Nernst-Plank equation, the molar flux ($\vec{N}_i$) of each specie i can be described as [29]:

$$\vec{N_i} = -D_i^{eff}\nabla C_i - z_i u_i^{eff} F C_i \nabla \phi_{a,l} \tag{4}$$

where C_i and z_i is the concentration and charge number of species i ($i = V^{2+}, V^{3+}, H^+, SO_4^{2-}$), respectively. F denotes Faradic constant. The effective diffusivity (D_i^{eff}) in the porous anode is given by the Bruggeman relation as [30]:

$$D_i^{eff} = {\varepsilon_a}^{1.5} D_i \tag{5}$$

where ε_a represents the porosity of anode and D_i represents the diffusion coefficient of specie i. The effective mobility (u_i^{eff}) in the porous anode follows the Nernst-Einstein relation as [31]:

$$u_i^{eff} = \frac{D_i^{eff}}{RT} \tag{6}$$

The mass conservation of each specie inside the anode at the transient state can be expressed as [32]:

$$\frac{\partial \varepsilon_a C_i}{\partial t} + \nabla \vec{N_i} = S_i \tag{7}$$

The source term S_i is the consumption/production rate of the species i resulted from the electrochemical reactions occurred in the porous anode, which is represented as [14]:

$$S_i = \frac{v_{a,i}}{n_a F} i_a \tag{8}$$

where v_a, n_a and i_a denote the stoichiometric coefficient, the number of participating electrons and the anode current density, respectively.

2.3.1.2. Charge transport. Inside the porous anode, the liquid fuel is considered as electrically neutral. Therefore, the electroneutrality can be described by ($i = V^{2+}, V^{3+}, H^+, SO_4^{2-}$) [33]:

$$\Sigma z_i C_i = 0 \tag{9}$$

During the cell operation, the charges transfer from the liquid phase to the solid electrode phase and generate current. Therefore, the charge conservation can be described as [14]:

$$i_a = \nabla \cdot \overrightarrow{i_{a,l}} = -\nabla \cdot \overrightarrow{i_{a,s}} \tag{10}$$

where $\overrightarrow{i_{a,l}}$ is the total ionic current due to ions transfer in the solutions ($i = V^{2+}, V^{3+}, H^+, SO_4^{2-}$), which is given by [14]:

$$\overrightarrow{i_{a,l}} = F \sum z_i \vec{N_i} \tag{11}$$

while $\overrightarrow{i_{a,s}}$ represents the total electronic current as [14]:

$$\overrightarrow{i_{a,s}} = -\sigma_a^{eff} \nabla \phi_{a,s} \tag{12}$$

where $\phi_{a,s}$ and σ_a^{eff} are the electric potential and effective electronic conductivity of anode, respectively. The σ_a^{eff} is calculated by the Bruggeman correction as [33]:

$$\sigma_a^{eff} = (1 - \varepsilon_a)^{\frac{3}{2}} \sigma_a \tag{13}$$

where σ_a is the electronic conductivity of the anode.

2.3.2. Cathode

2.3.2.1. Mass transport. At the cathode side, the diluted species approximation was used to describe the species transport. The air is diffused through the porous CDL to the CCL and the oxygen flux ($\vec{N}_{O_2}$) is defined by Fick's law [34]:

$$\overrightarrow{N_{O_2}} = -D_{O_2}^{eff} \nabla C_{O_2} \tag{14}$$

where C_{O_2} is the concentration of oxygen. The effective diffusivity $D_{O_2}^{eff}$ is given by the Bruggeman relation as [30]:

$$D_{O_2}^{eff} = \varepsilon_{ccl/cdl}^{\frac{3}{2}} D_{O_2} \tag{15}$$

where $\varepsilon_{ccl/cdl}$ represents the porosity of the CCL or CDL and D_{O_2} represents the diffusion coefficient of oxygen. The mass conservation at cathode side is given by:

$$\frac{\partial \varepsilon_{ccl/cdl} C_{O_2}}{\partial t} + \nabla \overrightarrow{N_{O_2}} = S_{O_2} \tag{16}$$

where the source term (S_{O_2}) can be represented as [35]:

$$S_{O_2} = \frac{v_{O_2} i_c}{n_c F} \tag{17}$$

where v_{O_2}, n_c and i_c denote the stoichiometric coefficient, the number of participating electrons and the cathode current density, respectively.

It is worth mentioning that when pure oxygen is used, the cathode is assumed to be fully filled with oxygen, where the oxygen concentration in the CCL and CDL are expressed as [34]:

$$C_{O_2} = C^0_{O_2,pure} \tag{18}$$

2.3.2.2. Charge transport. During the cell operation, the charge conservation in CCL is described by [14]:

$$i_c = \nabla \cdot \overrightarrow{i_{c,l}} = -\nabla \cdot \overrightarrow{i_{c,s}} \tag{19}$$

where $\overrightarrow{i_{c,l}}$ is the total ionic current due to ions transfer, which is given by [14]:

$$\overrightarrow{i_{c,l}} = -\sigma_{ccl,l} \nabla \phi_{c,l} \tag{20}$$

where $\sigma_{ccl,l}$ and $\phi_{c,l}$ are the ionic conductivity and ionic potential of CCL, respectively. $\overrightarrow{i_{c,s}}$ is the total electronic current due to electron transfer in the solid CCL following the Ohm's law [14]:

$$\overrightarrow{i_{c,s}} = -\sigma_{ccl,s} \nabla \phi_{c,s} \tag{21}$$

where $\sigma_{ccl,s}$ and $\phi_{c,s}$ are the electronic conductivity and electric potential of CCL, respectively.

2.3.3. Proton exchange membrane

Since there is no reaction in the PEM, the ionic current ($\overrightarrow{i_m}$) transport across membrane is given as [14]:

$$\overrightarrow{i_m} = -\sigma_m \nabla \phi_m \tag{22}$$

where σ_m and ϕ_m are the ionic conductivity and ionic potential of the membrane, respectively. Furthermore, the conservation of charge in the membrane gives [14]:

$$\nabla \cdot \overrightarrow{i_m} = 0 \tag{23}$$

The proton flux ($\overrightarrow{N_{H^+}}$) through the membrane is expressed as [14]:

$$\overrightarrow{N_{H^+}} = \frac{\overrightarrow{i_m}}{F} = -\frac{\sigma_m}{F} \nabla \phi_m \tag{24}$$

2.3.4. Electrochemical kinetics

In the anode, the interfacial reaction kinetics between the anode surface and liquid e-fuel are governed by the Butler-Volmer equation [14]:

$$i_a = a_{v,a} i_{0,a} \left[\exp\left(\frac{\alpha_{a,a} F \eta_a}{RT} \right) - \exp\left(-\frac{\alpha_{a,c} F \eta_a}{RT} \right) \right] \tag{25}$$

where $a_{v,a}$ denotes the anode specific area. $\alpha_{a,a}$ and $\alpha_{a,c}$ is the anode anodic and cathodic charge transfer coefficient, respectively. η_a represents the anode overpotential. The anodic exchange current density is defined as [14]:

$$i_{0,a} = F k_a (C_{V^{2+}})^{\alpha_{a,a}} (C_{V^{3+}})^{\alpha_{a,c}} \tag{26}$$

where k_a is the rate constant for anode reaction. While in CCL, Tafel equation is adopted for the calculation of the cathode current density [34]:

$$i_c = a_{v,c} i_{0,c} \left(\frac{C^{ccl}_{O_2}}{C^{ref}_{O_2}} \right)^{\gamma_c} \exp\left(\frac{\alpha_c F \eta_c}{RT} \right) \tag{27}$$

$$\gamma_c \begin{cases} 0 & C^{ccl}_{O_2} > C^{ref}_{O_2} \\ 1 & C^{ccl}_{O_2} \le C^{ref}_{O_2} \end{cases} \tag{28}$$

where $a_{v,c}$ denotes the CCL specific area, $i_{0,c}$ represents the cathodic exchange current density, α_c denotes cathode charge transfer coefficient and η_c represents cathode overpotential. The reaction order (γ_c) is set to be zero when the oxygen concentration in the CCL ($C^{ccl}_{O_2}$) exceeds the reference concentration ($C^{ref}_{O_2}$). The overpotentials on anode and cathode are represented as [14]:

$$\eta_{a/c} = \phi_{a/c,s} - \phi_{a/c,l} - E_{a/c} \tag{29}$$

where the anode equilibrium potential (E_a) is defined by the Nernst equation as [14,29]:

$$E_a = E^0_a + \frac{RT}{F} \ln\left(\frac{C_{V^{3+}}}{C_{V^{2+}}} \right) \tag{30}$$

In the meanwhile, the cathode equilibrium potential (E_c) is defined as:

$$E_c = E^0_c \tag{31}$$

where E^0_a and E^0_c is the equilibrium potentials of the anode and cathode half reactions, respectively.

2.3.5. Boundary conditions

It is assumed that no inward flux exists at the outer wall of the domain, which can be expressed by:

$$-\overrightarrow{n} \cdot \overrightarrow{N_i} = 0 \tag{32}$$

In the anode, at the tank/current collector interface, the concentration of species i is assumed to be constant, which is expressed as [34]:

$$C_i = C^0_i \tag{33}$$

where C^0_i is the initial concentration of species i. Similarly, at the interface between the cathode current collector and outside, the oxygen concentration is assumed to be constant as [34]:

$$C_{O_2} = C^0_{O_2} \tag{34}$$

where $C^0_{O_2}$ is the initial concentration of oxygen.

At the electrode/membrane interfaces, the ionic potential is assumed to be continuous, which can therefore be expressed as [14]:

$$\phi_{a/c,l} - \phi_m = 0 \tag{35}$$

Moreover, the flux of species at the anode/membrane interface are given as [14]:

$$\overrightarrow{N_i} = 0 \ (i \neq H^+) \tag{36}$$

$$\overrightarrow{N_{H^+}} = \frac{\overrightarrow{i_{a,l}}}{F} \tag{37}$$

2.4. Computational settings

The model was solved by COMSOL using finite element method, where the tetrahedral structured mesh was generated with a total element number of 31,356. Before further study, the mesh-independence tests were also performed to validate the reliability of the developed model. Table 1, 2 and 3 summarize the parameters used

Table 1
Structural parameters.

Symbol	Description	Value	Unit	Ref.
h	Cell height	0.02	m	[36]
w	Cell width	0.02	m	[36]
δ_{ano}	Anode thickness	0.0015	m	[14]
δ_m	Membrane thickness	200	μm	[44]
δ_{cdl}	Thickness of CDL	260	μm	[45]
δ_{ccl}	Thickness of CCL	10	μm	[45]
ε_a	Porosity of anode	0.68	/	[46]
ε_{cdl}	Porosity of CDL	0.7	/	[47]
ε_{CCL}	Porosity of CCL	0.3	/	[47]
$a_{v,a}$	Specific area of the porous anode	16,200	m^{-1}	[44]
$a_{v,ccl}$	Specific area of the CCL	2×10^5	m^{-1}	[45]
σ_a	Electrical conductivity of the solid phase	1000	S m^{-1}	[44]
σ_m	Membrane conductivity	5.5	S m^{-1}	[34]
$\sigma_{cdl,s}$	Electrical conductivity of CDL	5000	S m^{-1}	[48]
$\sigma_{ccl,s}$	Electrical conductivity of CCL	2000	S m^{-1}	[48]
$\sigma_{ccl,l}$	Ionic conductivity of CCL	3.05	S m^{-1}	[14]

Table 2
Properties and parameters.

Symbol	Parameter description	Value	Unit	Ref.
$C^0_{V^{2+}}$	Initial concentration of V^{2+}	1000	mol m^{-3}	[36]
$C^0_{V^{3+}}$	Initial concentration of V^{3+}	200	mol m^{-3}	[36]
$C^0_{H^+}$	Initial concentration of H^+	6000	mol m^{-3}	[36]
$C^0_{O_2,\ air}$	Initial concentration of O_2 in air	8.584	mol m^{-3}	[34]
$C^0_{O_2,\ pure}$	Initial concentration of pure O_2	40.876	mol m^{-3}	[34]
$C^{ref}_{O_2}$	Reference concentration of O_2	40.876	mol m^{-3}	[34]
$D_{V^{2+}}$	Diffusion coefficient of V^{2+}	2.4×10^{-10}	$m^2\ s^{-1}$	[49]
$D_{V^{3+}}$	Diffusion coefficient of V^{3+}	2.4×10^{-10}	$m^2\ s^{-1}$	[49]
D_{H^+}	Diffusion coefficient of H^+	9.3×10^{-9}	$m^2\ s^{-1}$	[49]
$D_{SO_4^{2-}}$	Diffusion coefficient of SO_4^{2-}	1.07×10^{-9}	$m^2\ s^{-1}$	[49]
D_{O_2}	Diffusion coefficient of O_2	2.5×10^{-5}	$m^2\ s^{-1}$	[50]

Table 3
Electrochemical parameters.

Symbol	Description	Value	Unit	Ref.
$\alpha_{a,a}$	Anode anodic charge transfer coefficient	0.4	/	Estimated
$\alpha_{a,c}$	Anode cathodic charge transfer coefficient	0.6	/	Estimated
α_c	Cathode charge transfer coefficient	0.5	/	[34]
k_a	Anode reaction rate constant	7×10^{-8}	m s^{-1}	[46]
$i_{0,c}$	Cathodic exchange current density	0.11	A m^{-2}	[51]
E^0_a	Anode equilibrium potential	-0.26	V	[36]
E^0_c	Cathode equilibrium potential	1.23	V	[36]

during model development.

3. Results and discussion

3.1. Model validation

To begin with, the model is first validated by comparing the numerical results with experimental data. As reported, the experiment was conducted using a homemade passive fuel cell where the e-fuel composed of V^{2+} ions in 3.0 M H_2SO_4 and ambient air are supplied as reactants [36]. Using the same operating parameters, the simulation results correlate well with the experimental data under a wide range of e-fuel concentrations from 0.2 to 1.0 M V^{2+} ions as presented in Fig. 2 **(a)**, which thereby demonstrates the accuracy of the model developed. A further analysis of the simulation results shows that, the cell performance is found to be significantly enhanced with the increment of the e-fuel concentration. Such a change can be traced back to the presence of more V^{2+} ions on the electrode surface (Fig. 2**(b)**). When examined under the same current density, the concentration of V^{2+} ions within anode is found to increase with the e-fuel concentration, which enables a lower concentration polarization loss and further ensures a better cell performance [37]. Moreover, the performance boost can be ascribed to the improved mass transport due to the enhanced diffusion process. It is also worthy noticing that irrespective of the e-fuel composition used, when the discharging current density approaches the respective maximum current density, as represented at point B to F, the concentrations of V^{2+} ions in the electrode are all identical and extremely low, which thereby demonstrates the limited mass transport to be the major reason restricting the cell performance. However, undeniably, the deviation in the cell voltage between the model and experiment results becomes relatively larger as the liquid e-fuel concentration gets higher and the discharging current density rises. Such a difference is considered to arise from some of the assumptions made during modeling. For instance, the assumption of no liquid e-fuel crossover through the membrane ignored the possible mixed overpotential loss induced, while the exclusion of liquid water generated during cell operation disregards the negative impacts associated with the water flooding issue, which therefore make the model to be unable of achieving a perfect fitting with the experimental results [38,39].

3.2. Effect of anode thickness

As a key structural parameter, the anode thickness has a great impact on cell performance. On the one hand, a thicker anode could ensure a larger surface area and thereby offer more reactive sites for the electrochemical reaction to lower the polarization loss. On the other hand, the larger anode thickness may lead to a longer path for the species transport and thereby result in a higher mass transfer resistance to limit the cell performance [40]. Therefore, to examine its actual influence, using the model developed, the effects of anode thickness are studied here. As in Fig. 3**(a)**, the cell using five different anode thicknesses including 1.0, 1.5, 2.0, 2.5, and 3.0 mm have been simulated, where the cell performance is found to be improved with the anode thickness. More detailly, both the cell voltage and maximum current density boost as the anode thickness increases. Notably, the fuel cell using 3.0 mm anode exhibits a maximum current density of 280 mA cm^{-2}, which thereby demonstrates the significant role of anode thickness in determining the cell performance. Furthermore, it is noted that when examined under the same current density, the cell with a thicker anode is found to present a higher V^{2+} ions concentration distribution (point A in Fig. 3**(b)**), which thereby allows the cell to be with better performance by alleviating the concentration polarization loss. However, it should be noted that the increment of anode thickness would on the other hand results in larger ohmic resistance, which could eventually lead to a large ohmic polarization and degrades the cell performance [14].

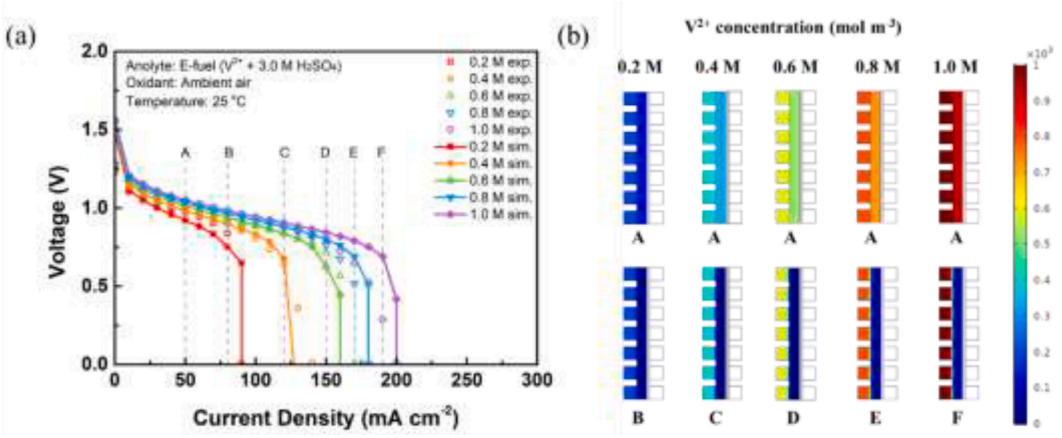

Fig. 2. (a) Model validation; (b) Concentration distribution of V^{2+} ions at the anode at different discharging current densities.

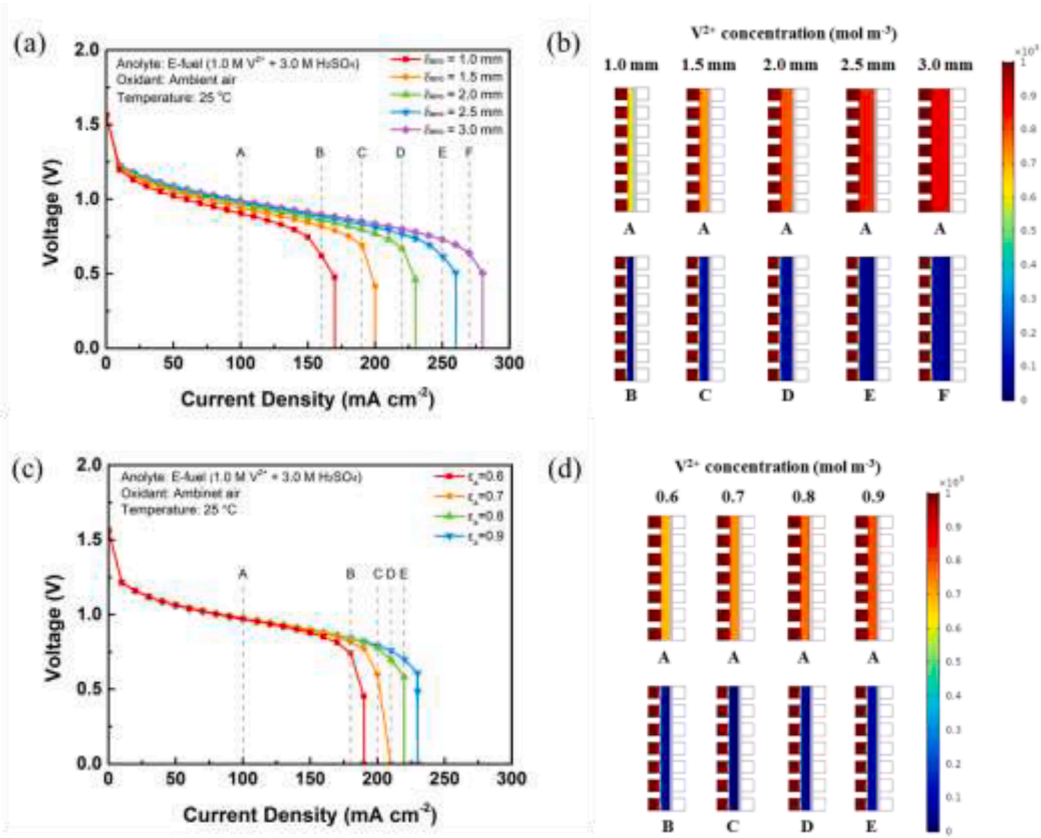

Fig. 3. Effects of the anode thickness on (a) the cell performance and (b) the concentration distribution of V^{2+} ions at the anode at different discharging current densities; and effects of anode porosity on (c) the cell performance and (d) concentration distribution of V^{2+} ions at the anode at different discharging current densities.

3.3. *Effect of anode porosity*

The transport of reactive species inside this fuel cell mainly follows diffusion and migration. Therefore, in addition to the anode thickness, the anode porosity is also a key parameter that influences the delivery of electroactive species to the reactive surface and further determines the cell performance. Here, different anode porosities of 0.6, 0.7, 0.8, and 0.9 have been used for numerical studies to analyze its effects (Fig. 3**(c)**). It shows that, at the low to middle current density region, the cell voltages using anodes of different porosities are similar. This may be attributed to the fact that the reaction kinetic of V^{2+} ions on carbon-based anode is rapid, so that the effect of increasing electrode porosity does not have any obvious effect on the cell activation loss. While in contrast, the cell maximum current density is found to increase with the anode porosity, where it rises from 190 mA cm^{-2} (0.6) to 230 mA cm^{-2} (0.9) as shown in point B to E in Fig. 3**(c)**. Such a phenomenon is considered to be attributed to the higher reactants permeability as a result of larger anode porosity, which thereby ensures the electrode surface to be with higher e-fuel concentration. At 180 mA cm^{-2} (point B in Fig. 3**(d)**), for example, the concentration of V^{2+} ions in the anode with a porosity of 0.9 is much higher than that with a porosity of 0.6, which therefore justifies the improved reactant mass transport. It is due to this enhanced mass/charge transport inside the fuel cell, a lower concentration polarization loss inside the porous anode is achieved

which thereby lowers the overpotentials and enhances the cell performance [34]. Nevertheless, it is worth mentioning that, a larger anode porosity would also result in less solid region, which thereby would hamper the conduction of electrons and eventually lead to a large cell ohmic resistance [41].

3.4. Effect of cathode catalyst layer thickness

Similar to the porous anode, the CCL is also an essential part that not only provides reactive sites for the cathode oxygen reduction reaction, but also influences the oxygen transport. Hence, the CCL thickness is also pivotal to the cell performance. In this section, numerical model is used to study the effects of CCL thickness and the results are shown in Fig. 4**(a)**. It suggests that the cell voltage gets higher with the increment of the CCL thickness, which indicates an improved overall cell performance. In more detail, for instance, the open-circuit voltage of the cell can be seen to increase to 1.65 V as the cathode catalyst thickness increases to 100 μm. Such a boost in the cell performance is due to the fact that a thicker CCL can provide more reactive sites and thereby lowers the cathode overpotential to achieve a higher cell voltage [35]. However, it is worth mentioning that, the thicker CCL can also impede the oxygen transport due to the lengthened channel and further show a negative effect on the cell performance eventually [42].

3.5. Effect of the oxygen concentration

During cell operation, oxygen molecules are needed to transport through the CDL to reach the CCL for participating in the reactions. Hence, the oxygen concentration is another major factor which is critical for the cell performance. As presented in Fig. 4**(b)**, the cell fed with the pure oxygen is found to achieve a higher cell voltage in comparison to its performance when fed with ambient air. Such a result is due to the presence of more oxidant molecules within the cathode by using pure oxygen, which thereby lowers the cathode overpotential. However, it is also found that, using both the pure oxygen and the ambient air as oxidant, the cell exhibits the same maximum current density. On top of that, as presented in Fig. 4**(c)**, even when ambient air is fed, the oxygen concentration gradient from the outlet to the CCL remains small in spite of the discharging current density approaching the maximum current density, which thereby suggests the oxygen concentration be sufficient throughout the whole test. In contrast, at near the maximum current density, the concentration of electroactive species inside porous anode is found to be extremely low. Such a phenomenon thus indicates that the major reason limiting the fuel cell performance arises from the insufficient electroactive species inside the porous anode, while the oxidant due to the relatively high diffusion coefficient of gaseous oxygen is not the primary cause.

3.6. Effect of anodic/cathodic exchange current density

Besides the various structural parameters, the electrocatalytic activity also affects the system performance. The exchange current density is an indicator of the electrode electrocatalytic activity, which can reflect the electrochemical kinetics of the reactions [43]. Therefore, here, the effects of exchange current density on the cell performance are investigated (Fig. 5), where their increments are found to boost the cell performance. For instance, the cell voltage is found to increase as the cathodic exchange current density rises, demonstrating the importance of cathode catalytic reactivity towards the cell performance. More detailly, at 50 mA cm^{-2}, the cell voltage is found to elevate to 1.30 V as the cathodic exchange current density is increased to 100 A m^{-2}, proving an improved cell performance due to lowered cathode overpotential. Similar performance enhancement is also found with the increase of anodic exchange current density, where a lower anode overpotential results in a better cell performance. Overall, the highest anodic and cathodic exchange current density are proved to offer the best cell performance. Therefore, it is believed that, increasing the exchange current densities via developing porous anode and cathode catalyst materials with better catalytic reactivity should be regarded as an efficient approach to boost the fuel cell performance.

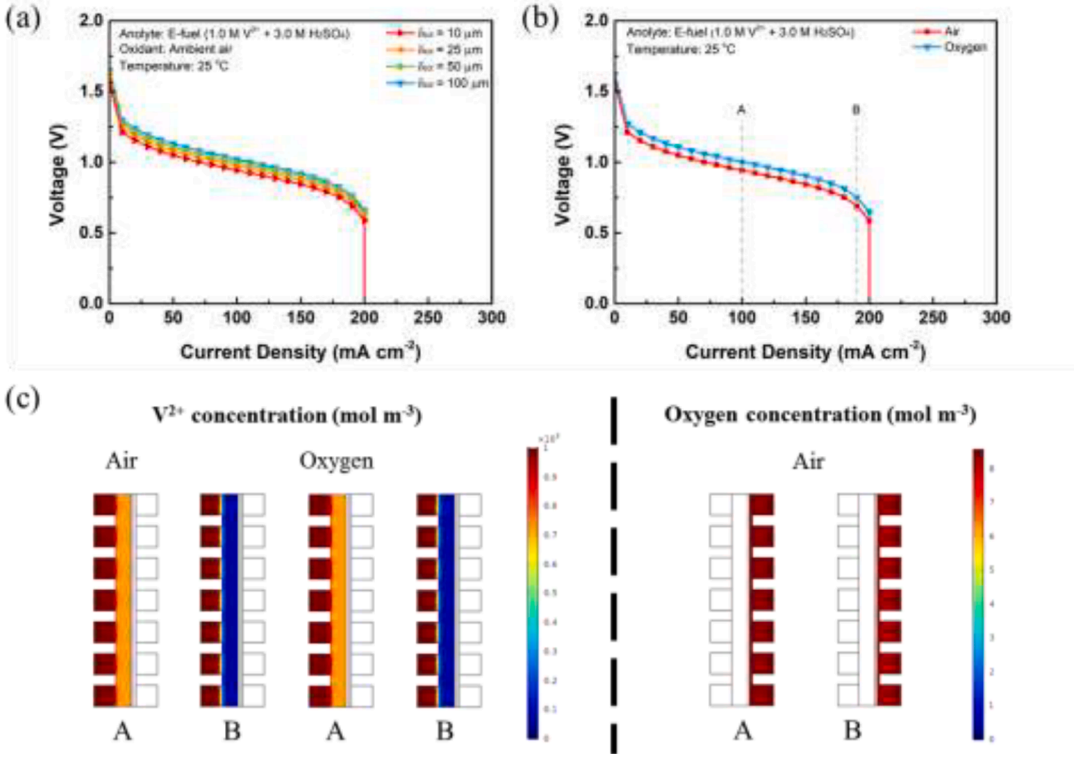

Fig. 4. Effects of (a) the CCL thickness and (b) oxygen concentration on the cell performance; and (c) concentration distributions of V^{2+} ions at the anode and oxygen at the cathode at different discharging current densities.

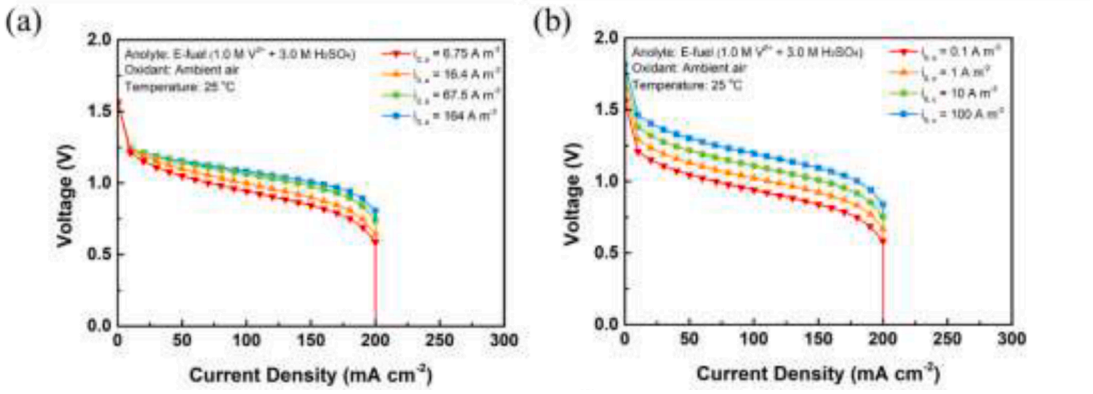

Fig. 5. Effects of the (a) anodic and (b) cathodic exchange current densities on the cell performance.

4. Summary

In this work, a 2D transient model for the liquid fuel cell fed with the e-fuel has been developed. The numerical data shows a superior agreement with experimental results, which not only demonstrates its accuracy but also helps to analyze the concentration distribution of reactive species within the cell, showing the limited mass transport of e-fuel to be the major reason restricting the cell performance. In addition, various structural parameters such as the anode thickness, anode porosity, and CCL thickness are also studied, where their increment are all found to boost the cell performance. Meanwhile, the effect of oxygen concentration is also examined, where the usage of oxidant with a higher oxygen concentration is found to be able of achieving a higher cell voltage while the predominant reason limiting the operational current density range is found to be arising from the anode side due to the slow e-fuel transport. Furthermore, the anodic and cathodic exchange current densities are also demonstrated to influence the cell performance due to the significant roles of electrodes catalytic reactivity in influencing the anode and cathode overpotential. In the future, to achieve further performance enhancement, it is necessary for the system to overcome the current mass transport limitations, which can be realized by using strategies such as modifying the fuel compositions to ensure lower fuel viscosity. It is also believed that with the development of catalysts with excellent electrocatalytic reactivity especially for the oxygen reduction reaction, the cell performance can be further boosted and finally achieve the commercialization of the system.

Declaration of Competing Interest

There are no conflicts to declare.

Data availability

Data will be made available on request.

Acknowledgement

The work described in this paper was supported by a grant from the Research Grant Council of the Hong Kong Special Administrative Region, China (Project No. T23–601/17-R) and a grant from the Research Institute for Smart Energy (RISE) at The Hong Kong Polytechnic University (Q-CDA4).

References

[1] Singla MK, Nijhawan P, Oberoi AS. Hydrogen fuel and fuel cell technology for cleaner future: a review. Environ Sci Pollut Res 2021;28:15607–26.
[2] Wang J, Wang H, Fan Y. Techno-economic challenges of fuel cellcommercialization. Engineering 2018;4:352–60.
[3] Sazali N, Wan Salleh WN, Jamaludin AS, Mhd Razali MN. New perspectives on fuel cell technology: A brief review. Membranes 2020;(10):99.
[4] Shaari N, Kamarudin SK, Bahru R, Osman SH, Md Ishak NAI. Progress and challenges: Review for direct liquid fuel cell. Int J Energy Res 2021;45:6644–88.
[5] Suraparaju SK, Natarajan SK, Karthikeyan P. A succinct review on fuel cells. IOP Conference Series: Earth and Environmental Science 2019:012012.
[6] Scofield ME, Liu H, Wong SS. A concise guide to sustainable PEMFCs: recent advances in improving both oxygen reduction catalysts and proton exchange membranes. Chem Soc Rev 2015;44:5836–60.
[7] Whiston MM, Lima Azevedo IM, Litster S, Samaras C, Whitefoot KS, Whitacre JF. Hydrogen storage for fuel cell electric vehicles: Expert elicitation and a levelized cost of driving model. Environ Sci Technol 2020;55:553–62.
[8] Ong B, Kamarudin S, Basri S. Direct liquid fuel cells: A review. Int J Hydrogen Energy 2017;42:10142–57.
[9] Kumar P, Dutta K, Das S, Kundu PP. An overview of unsolved deficiencies of direct methanol fuel cell technology: factors and parameters affecting its widespread use. Int J Energy Res 2014;38:1367–90.
[10] Abdullah S, Kamarudin S, Hasran U, Masdar M, Daud W. Modeling and simulation of a direct ethanol fuel cell: An overview. J Power Sources 2014;262:401–6.
[11] Basri S, Kamarudin S, Daud W, Yaakub Z. Nanocatalyst for direct methanol fuel cell (DMFC). Int J Hydrogen Energy 2010;35:7957–70.
[12] Shi X, Huo X, Ma Y, Pan Z, An L. Energizing fuel cells with an electrically rechargeable liquid fuel. Cell Reports Phys Sci 2020;1:100102.
[13] Shi X, Huo X, Esan OC, Ma Y, An L, Zhao T. A liquid e-fuel cell operating at− 20° C. J Power Sources 2021;506:230198.
[14] Esan OC, Shi X, Su X, Dai Y, An L, Zhao T. A computational model of a liquid e-fuel cell. J Power Sources 2021;501:230023.
[15] Abdullah S, Kamarudin SK, Hasran UA, Masdar M, Daud WRW. Electrochemical kinetic and mass transfer model for direct ethanol alkaline fuel cell (DEAFC). J Power Sources 2016;320:111–9.
[16] Oh K, Yoo H, Ko J, Won S, Ju H. Three-dimensional, transient, nonisothermal model of all-vanadium redox flow batteries. Energy 2015;81:3–14.
[17] Pham TT, Mollaamin F, Monajjemi M, Dang CM. A review of 2019 fuel cell technologies: modelling and controlling. Int J Nanotechnol 2020;17:498–513.
[18] Esan OC, Shi X, Pan Z, Huo X, An L, Zhao T. Modeling and simulation of flow batteries. Adv Energy Mater 2020;10:2000758.
[19] Pang Y, Wang Y. Water spatial distribution in polymer electrolyte membrane fuel cell: Convolutional neural network analysis of neutron radiography. Energy and AI 2023;14:100265.
[20] Legala A, Zhao J, Li X. Machine learning modeling for proton exchange membrane fuel cell performance. Energy and AI 2022;10:100183.
[21] Yang Y, Liang YC. Modelling and analysis of a direct methanol fuel cell with under-rib mass transport and two-phase flow at the anode. J Power Sources 2009;194:712–29.
[22] Ye Q, Zhao T, Xu C. The role of under-rib convection in mass transport of methanol through the serpentine flow field and its neighboring porous layer in a DMFC. Electrochim Acta 2006;51:5420–9.
[23] Kulikovsky A. A model for mixed potential in direct methanol fuel cell cathode. Electrochim Acta 2012;62:185–91.
[24] Liu F, Wang CY. Mixed potential in a direct methanol fuel cell: modeling and experiments. J Electrochem Soc 2007;154:B514.
[25] Gerteisen D. Transient and steady-state analysis of catalyst poisoning and mixed potential formation in direct methanol fuel cells. J Power Sources 2010;195:6719–31.
[26] Vasile NS, Videla AHM, Simari C, Nicotera I, Specchia S. Influence of membrane-type and flow field design on methanol crossover on a single-cell DMFC: An experimental and multi-physics modeling study. Int J Hydrogen Energy 2017;42:27995–8010.
[27] Wang SJ, Huo WW, Zou ZQ, Qiao YJ, Yang H. Computational simulation and experimental evaluation on anodic flow field structures of micro direct methanol fuel cells. Appl Therm Eng 2011;31:2877–84.

[28] Sudaroli BM, Kolar AK. Experimental and numerical study of serpentine flow fields for improving direct methanol fuel cell performance. Fuel cells 2015;15:826–38.
[29] Knehr K, Agar E, Dennison C, Kalidindi A, Kumbur E. A transient vanadium flow battery model incorporating vanadium crossover and water transport through the membrane. J Electrochem Soc 2012;159:A1446.
[30] Ismail M, Ingham D, Hughes K, Ma L, Pourkashanian M. Effective diffusivity of polymer electrolyte fuel cell gas diffusion layers: an overview and numerical study. Int J Hydrogen Energy 2015;40:10994–1010.
[31] Zhou X, Zhao T, An L, Zeng Y, Yan X. A vanadium redox flow battery model incorporating the effect of ion concentrations on ion mobility. Appl Energy 2015; 158:157–66.
[32] Won S, Oh K, Ju H. Numerical analysis of vanadium crossover effects in all-vanadium redox flow batteries. Electrochim Acta 2015;177:310–20.
[33] Sathisha H, Dalal A. Two-Dimensional Unsteady Simulation of All-Vanadium Redox Flow Battery. J Therm Sci Eng Appl 2016;8.
[34] An L, Chai Z, Zeng L, Tan P, Zhao T. Mathematical modeling of alkaline direct ethanol fuel cells. Int J Hydrogen Energy 2013;38:14067–75.
[35] Su X, Pan Z, An L, Yu Y. Mathematical modeling of direct formate fuel cells incorporating the effect of ion migration. Int J Heat Mass Transf 2021;164:120629.
[36] Shi X, Dai Y, Esan OC, Huo X, An L, Zhao T. A passive fuel cell fed with an electrically rechargeable liquid fuel. ACS Appl Mater Interfaces 2021;13: 48795–800.
[37] Yuan Z, Yang J, Zhang Y, Zhang X. The optimization of air-breathing micro direct methanol fuel cell using response surface method. Energy 2015;80:340–9.
[38] Shi X, Huo X, Esan OC, Dai Y, An L, Zhao T. Manipulation of electrode composition for effective water management in fuel cells fed with an electrically rechargeable liquid fuel. ACS Appl Mater Interfaces 2022;14:18600–6.
[39] Shi X, Esan OC, Huo X, Ma Y, Pan Z, An L, et al. Polymer electrolyte membranes for vanadium redox flow batteries: fundamentals and applications. Prog Energy Combust Sci 2021;85:100926.
[40] Kumar S, Jayanti S. Effect of electrode intrusion on pressure drop and electrochemical performance of an all-vanadium redox flow battery. J Power Sources 2017;360:548–58.
[41] Larbi B, Alimi W, Chouikh R, Guizani A. Effect of porosity and pressure on the PEM fuel cell performance. Int J Hydrogen Energy 2013;38:8542–9.
[42] Matar S, Liu H. Effect of cathode catalyst layer thickness on methanol cross-over in a DMFC. Electrochim Acta 2010;56:600–6.
[43] Pan Z, Bi Y, An L. Mathematical modeling of direct ethylene glycol fuel cells incorporating the effect of the competitive adsorption. Appl Therm Eng 2019;147: 1115–24.
[44] Ali E, Kwon H, Choi J, Lee J, Kim J, Park H. A numerical study of electrode thickness and porosity effects in all vanadium redox flow batteries. J Energy Storage 2020;28:101208.
[45] Ghasabehi M, Ashrafi M, Shams M. Performance analysis of an innovative parallel flow field design of proton exchange membrane fuel cells using multiphysics simulation. Fuel 2021;285:119194.
[46] Oh K, Won S, Ju H. A comparative study of species migration and diffusion mechanisms in all-vanadium redox flow batteries. Electrochim. Acta 2015;181: 238–47.
[47] Xue YQ, Guo H, Shang HH, Ye F, Ma CF. Simulation of mass transfer in a passive direct methanol fuel cell cathode with perforated current collector. Energy 2015; 81:501–10.
[48] Zhang S, Beale S, Reimer U, Andersson M, Lehnert W. Polymer electrolyte fuel cell modeling-A comparison of two models with different levels of complexity. Int J Hydrogen Energy 2020;45:19761–77.
[49] Wandschneider F, Küttinger M, Noack J, Fischer P, Pinkwart K, Tübke J, et al. A coupled-physics model for the vanadium oxygen fuel cell. J Power Sources 2014; 259:125–37.
[50] Chen R, Zhao T. Mathematical modeling of a passive-feed DMFC with heat transfer effect. J Power Sources 2005;152:122–30.
[51] Cai W, Li S, Feng L, Zhang J, Song D, Xing W, et al. Transient behavior analysis of a new designed passive direct methanol fuel cell fed with highly concentrated methanol. J Power Sources 2011;196:3781–9.